Applied Energy 329 (2023) 120283

Contents lists available at ScienceDirect

Applied Energy

journal homepage: www.elsevier.com/locate/apenergy

Intrusive and non-intrusive early warning systems for thermal discomfort by analysis of body surface temperature☆

Ziyang Wang *, Ryuji Matsuhashi, Hiroshi Onodera

Department of Electrical Engineering and Information Systems, The University of Tokyo, Tokyo 113-8656, Japan

GRAPHICAL ABSTRACT

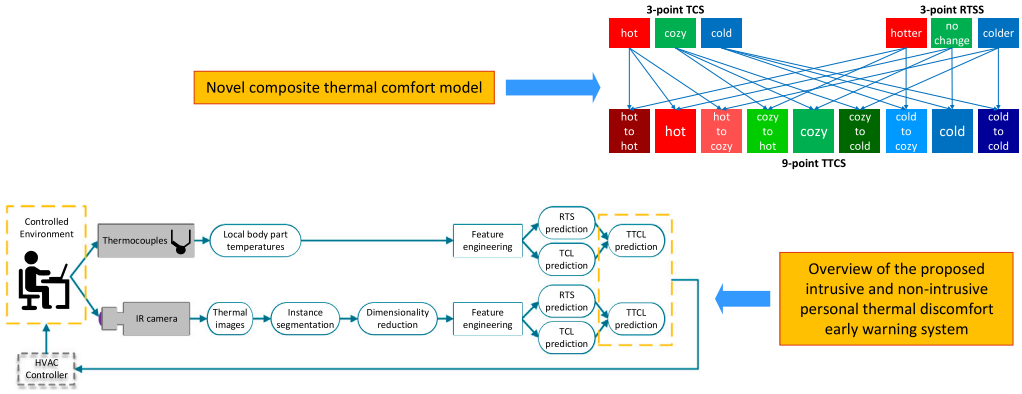

ARTICLE INFO

Keywords:
Thermal comfort
Energy conservation
Relative thermal sensation
Physiological index
Infrared thermography
Machine learning

ABSTRACT

Buildings consume huge amounts of energy for the thermal comfort maintenance of the occupants. Real-time thermal comfort assessment is both important in the occupants' thermal comfort optimization and energy conservation in the building sector. Existing thermal comfort studies mainly focus on the real-time assessment of the occupant's current thermal comfort. Nonetheless, in the transient thermal environment, the occupant's current thermal comfort is not steady and changes moment by moment. Hence, a prediction error will be elicited if we merely assess the occupant's current thermal comfort. To address this problem, it is crucial to comprehend the occupant's real-time thermal sensation trend in the transient thermal environment. A novel thermal sensation index that directly accounts for an occupant's current thermal sensation trend is investigated in this study. By integrating the novel thermal sensation index into an ordinary thermal comfort model, a novel composite thermal comfort model is derived, which can simultaneously address the occupant's current thermal comfort and current thermal sensation trend. Next, by utilizing machine learning classifications, we propose the intrusive and non-intrusive assessment methods of the composite thermal comfort model by analysis of the skin/clothing temperatures of ten local body parts measured by thermocouple thermometers and upper body thermal images measured by a low-cost portable infrared camera. The intrusive method reached a mean accuracy of 59.7% and 52.0% in Scenarios I and II, respectively; the non-intrusive method reached a mean accuracy of 45.3% and 42.7% in Scenarios I and II, respectively. The composite thermal comfort model provides a thermal discomfort early warning mechanism and contributes to energy conservation in the building sector.

☆ The short version of the paper was presented at ICAE2021, Nov 29–Dec 5, 2021. This paper is a substantial extension of the short version of the conference paper.

* Corresponding author.
E-mail address: wangziyang@g.ecc.u-tokyo.ac.jp (Z. Wang).

https://doi.org/10.1016/j.apenergy.2022.120283
Received 22 May 2022; Received in revised form 26 October 2022; Accepted 31 October 2022
Available online 15 November 2022

Nomenclature

Abbreviations

ASHRAE	American Society of Heating, Refrigerating and Air-conditioning Engineers
HVAC	Heating, Ventilation and Air Conditioning
TSV	Thermal sensation vote
TCV	Thermal comfort vote
TP	Thermal preferences
PMV	Predicted Mean Vote
RTS	Relative Thermal Sensation
ATS	Absolute Thermal Sensation
TCL	Thermal Comfort Level
TTCL	Transient Thermal Comfort Level
RTSV	Relative Thermal Sensation Vote
ATSV	Absolute Thermal Sensation Vote
3-point RTSS	3-point Relative Thermal Sensation Scale
7-point ATSS	7-point Absolute Thermal Sensation Scale
3-point TCS	3-point Thermal Comfort Scale
9-point TTCS	9-point Transient Thermal Comfort Scale
ROI	Region of interest
YOLACT	You Only Look At CoefficienTs
PCA	Principal Component Analysis
CAE	Convolutional autoencoder
UMAP	Uniform Manifold Approximation and Projection for Dimension Reduction
MLP	Multilayer Perceptron
LBPT	Local body part temperatures
DRTP	Dimension-reduced thermal profiles

Variables

T_I	Air temperature in the inner chamber (°C)
T_E	Air temperature in the external environment (°C)
LT_t	LBPT at time t
$\overline{LT_t}$	Smoothed LBPT at time t
LTG_t	Gradients of the LBPT at time t
DP_t	DRTP at time t
$\overline{DP_t}$	Smoothed DRTP at time t
DPG_t	Gradients of the DRTP at time t

1. Introduction

Buildings account for over one-third of global final energy consumption [1] directly and indirectly, more than 50% of which is used for occupants' thermal comfort satisfaction through the Heating, Ventilation, and Air Conditioning (HVAC) systems [2]. Real-time thermal comfort assessment is both important in the occupants' thermal comfort optimization and energy conservation in the building sector. Thermal comfort is defined as "the condition of mind that expresses satisfaction with the thermal environment and is assessed by subjective evaluation" [3] by the American Society of Heating, Refrigerating and Air-Conditioning Engineers (ASHRAE) in the ASHRAE Standard 55-2017, indicating that thermal comfort is only determined by one's subjective judgment about the surrounding thermal environment. Survey-based methods require the occupants to give real-time personal thermal comfort via questionnaires, such as the thermal sensation vote (TSV), thermal comfort vote (TCV), thermal preferences (TP) [4], et cetera. In spite of the direct extraction of occupants' real-time thermal comfort, occupants have to continuously provide feedback through these methods.

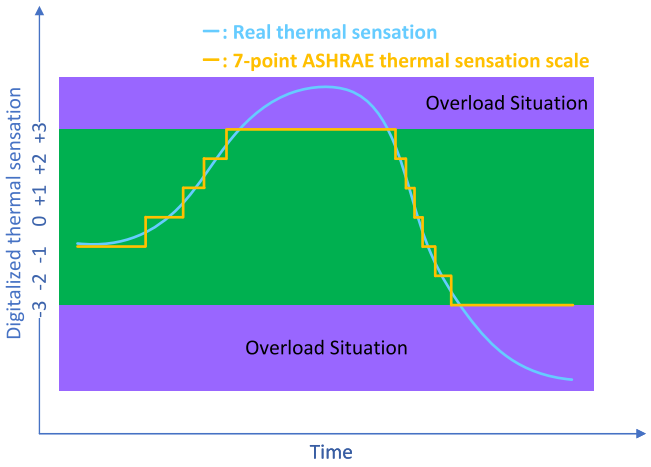

Fig. 1. Schematic illustration of the drawbacks of the ASHRAE 7-point thermal sensation scale.

Despite the extensive usage of the TSV/TCV/TP, these kinds of questionnaires have three major limitations, which are illustrated as follows. For instance, the American Society of Heating, Refrigerating and Air-Conditioning Engineers (ASHRAE) defined 7-point thermal sensation scale [3], expressed from −3 to +3 corresponding to the categories "cold", "cool", "slightly cool", "neutral", "slightly warm", "warm", and "hot", is widely used in a variety of thermal comfort studies. First, since the TSV/TCV/TP usually has a limited range, when an individual's real thermal sensation exceeds the upper limit or the lower limit, overload situations will occur, as illustrated in Fig. 1. Second, if we suppose individuals' real thermal sensation to be continuous, potential fine details will be lost when only using the TSV/TCV/TP since it is discrete, as illustrated in Fig. 1. Third, in existing thermal comfort studies, the voting interval of the TSV/TCV/TP was usually set to be a fixed value and sometimes cannot address the subtle changes or fine details and consequently incapable of making a precise assessment of thermal comfort (e.g., TSV: 5 min [5,6] or 1 min [7]; TCV interval: 15 min [8]; TP: 3 min [9], or 1 min [10]).

In the transient thermal environment, the occupant's current thermal comfort is not steady and changes moment by moment. For example, suppose an occupant who only wears a short sleeve walks out of a well-heated house in winter, the occupant may initially feel comfortably cool. However, there is a high possibility that the occupant would finally feel uncomfortably cold. On the contrary, suppose the occupant enters a sauna room, the occupant might initially feel comfortably warm. As time goes by, with the body absorbing too much heat, the occupant may finally feel uncomfortably hot. In other words, an occupant's thermal comfort could be "comfortable" at present, while after some time, it could possibly transition to "uncomfortably cold" or "uncomfortably hot" in the transient thermal environment. Hence, a prediction error will be elicited if we merely assess the occupant's current thermal comfort.

So far, scholars have done various research on assessing occupants' thermal comfort to eliminate continuous feedback. The most extensively used method is the Predicted Mean Vote (PMV) model [11], based on six factors: air temperature, mean radiant temperature, air velocity, relative humidity, metabolic rate, and clothing insulation, which can affect one's thermal sensation and comfort. The PMV model is an empirical formulas-based model that has the ability to predict the average thermal comfort of a large majority of people. However, this also means the PMV model cannot account for individual differences [12]. On the other hand, since it has been revealed that individual

differences in personal thermal comfort and the dynamic features could be reflected in some physiological indices (e.g., skin temperature [13–16], electrodermal activity [17], electroencephalogram [18,19], heart rate [20], core temperature [21], sweating loss [22]), existing thermal comfort studies have paid a lot attention to dynamic thermal comfort assessment in transient thermal environments by analysis of physiological indices and the occupants' limited TSV/TCV/TP data to construct personal thermal comfort models to eliminate continuous feedback from occupants. Wang [22] developed a thermo-regulatory model capable of predicting a subject's thermal sensation under transient conditions by analysis of sweating loss and skin temperature. Fiala [14] demonstrated that the skin temperature, head-core temperature, and the rate of change of skin temperature are responsible for dynamic thermal comfort modeling. Zhang [15] used the time derivatives of the skin and core temperatures for local thermal sensation prediction under transient conditions. Schellen [16] developed a dynamic thermal comfort model based on the discharge rate of thermoreceptor neurons transduced by a mathematical formula using skin and core temperature recordings as inputs, which has been shown applicable in transient conditions.

However, the problem is that existing studies on thermal comfort assessment in transient thermal environments mainly use the TSV/TCV/TP to gather data from occupants and merely focus on the assessment of current thermal comfort and none of them are capable of accounting for the thermal sensation trend directly (e.g., is the current thermal comfort transitioning from "comfortable" to "uncomfortably cold" or "uncomfortably hot" or staying unchanging?). In summary, there lacks a thermal sensation index that can directly account for the real-time thermal sensation trend. If the thermal sensation trend can be accurately assessed, it will make great contributions to the thermal comfort assessment in the transient thermal environment and provides an early warning mechanism for thermal discomfort.

It has been revealed that the human thermoregulation system adjusts heat exchange with the environment by regulating skin blood flow through the cutaneous vessels in regard to thermal stress (namely, heat or cold) [23,24]. Therefore, the temperature or infrared radiation of the skin or clothing surface could be monitored to assess thermal comfort as implemented in a variety of studies [8,9,22,25–31]. Existing studies have extensively investigated using infrared thermometer [8] or thermography [9,29–31] to measure skin/clothing temperatures of specific regions of interest (ROIs) on the human body surface and use them as features for real-time thermal comfort modeling by utilizing machine learning classification algorithms. Even though these ROI extraction based methods have shown promising results for real-time personalized thermal comfort assessment, the drawbacks are summarized as follows: (1) the infrared camera should be set to the direct front of the occupant for ROI extraction [9], which could be disturbing and decreases the user experience; (2) only a small portion (namely, the ROIs) of the occupant's thermal image can be used and thus causes extreme information loss since the area out of the ROIs was not taken into account, where a huge amount of potential latent information may exist; (3) it usually demands a higher resolution of the infrared camera to capture the much smaller ROIs than the whole body.

To address these challenges, in our preliminary work [32], we proposed a novel thermal sensation index, which exactly accounts for individual real-time thermal sensation trend and tentatively investigated its intrusive assessment method by analyzing the subjects' skin/clothing temperatures of ten local body parts measured by thermocouple thermometers. In [32], we designed a 40-min-long experiment in which indoor transient thermal environments were simulated in an environmental test lab for the subjects to give their real-time TSVs, which were recorded by the keyboard of the laptop computer. Actually, in [32], we also took the thermal images of the subjects' upper body through a low-cost portable infrared camera. In this paper, we investigate the non-intrusive assessment method of the novel thermal sensation index using the subjects' thermal images and improve its intrusive assessment method by analysis of the subjects' local body part temperatures (LBPT). The paper is organized as follows. The proposed novel thermal sensation index, which accounts for the thermal sensation trend, is presented in Section 2. Section 3 illustrates the details of the experimental thermal conditions and data collection procedures. Section 4 shows the results and the performance metrics, as well as discusses the limitations of this study and illustrates the potential real-world applications of the presented novel thermal comfort model. Finally, Section 5 concludes the paper.

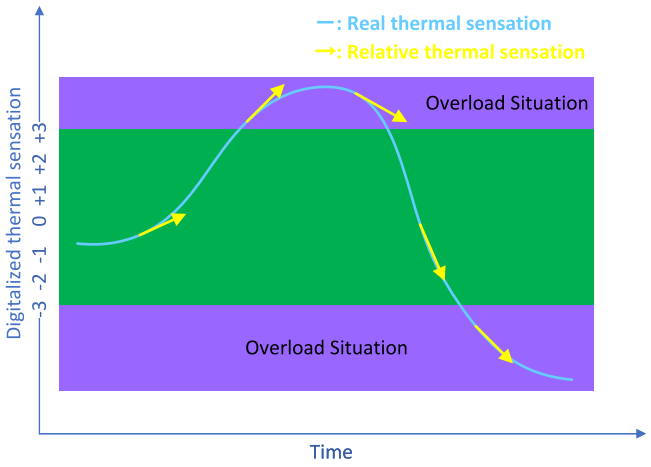

Fig. 2. Schematic illustration of the Relative Thermal Sensation (RTS).

2. Methodology

In order to account for the thermal sensation trend, we proposed a novel thermal sensation index, the Relative Thermal Sensation (RTS), which accounts for the real-time thermal sensation trend, and presented a composite thermal comfort model in [32]. For our explorations, we designed an experiment (see Section 3) in order to measure the subjects' LBPT and monitor the subjects' upper body thermal images during heating and cooling transient thermal conditions while collecting subjective TSVs. To make full use of the thermal information in the thermal images, instead of extracting the temperature of specific ROIs in the subjects' thermal images, in this study, we investigate using an instance segmentation algorithm to extract the subjects' thermal profiles. Then, a dimensionality reduction algorithm was applied to the thermal profiles to perform feature extraction. Next, feature engineering was applied to the LBPT and the dimension-reduced thermal profiles (DRTP) separately to generate multiple feature sets. Finally, machine learning classifications were carried out to evaluate the performance of each feature set. The whole learning framework is illustrated in Fig. 8.

2.1. Novel thermal comfort model

2.1.1. Relative Thermal Sensation

$$f(t) = f(t_0) + \frac{f'(t_0)}{1!}(t - t_0) + \frac{f''(t_0)}{2!}(t - t_0)^2 + \dots, \tag{1}$$

$$f(t) \approx f(t_0) + f'(t_0)(t - t_0) \tag{2}$$

Compared to the discrete ASHRAE 7-point thermal sensation scale, in this study, thermal sensation is considered to be a continuously infinitely differentiable function $f(t)$ of time t, where $f(t) > 0$ denotes hot sensation, $f(t) < 0$ denotes cold sensation, $f(t) = 0$ denotes neutral thermal sensation. The larger its absolute value $|f(t)|$, the greater the degree of hotness or coldness. Then at time t_0, the Taylor series form of $f(t)$ is shown in Eq. (1).

The linear approximation of $f(t)$ for t near t_0 is shown in Eq. (2) according to Taylor's theorem. At the right side of Eq. (2), the first term $f(t_0)$ is the exact thermal sensation degree at t_0. The coefficient of the second term $f'(t_0)$, describing the gradient of the thermal sensation at t_0, is precisely defined as the RTS at t_0 [32]. To gather the RTS reported by the occupants and for the sake of simplification, the 3-point Relative Thermal Sensation Scale (3-point RTSS) for the RTS assessment was proposed in [32], which consists of three categories "colder" (−1), "no change" (0), and "hotter" (+1), each category in which is called a Relative Thermal Sensation Vote (RTSV). The RTSV is defined as "colder" when the occupant's current thermal sensation is lower than the latest thermal sensation numerically (when $f'(t) < 0$); the RTSV is defined as "hotter" when the occupant's current thermal sensation is higher than the latest thermal sensation numerically (when $f'(t) > 0$); the RTSV is defined as "no change" when the occupant's current thermal sensation is equal to the latest thermal sensation numerically (when $f'(t) = 0$). By such a definition, the RTS forms another dimension of thermal comfort, and the 3-point RTSS can serve as a complementary thermal sensation scale for the traditional ASHRAE 7-point thermal sensation scale for the thermal comfort assessment in the transient thermal environment. Fig. 2 shows the illustration of the RTS. In Fig. 2, the blue curve indicates the real thermal sensation ($f(t)$). The yellow arrows are the tangents of the blue curve, which precisely illustrate the RTS ($f'(t)$). Furthermore, it is worth mentioning that the "hotter" RTS covers not only the transition from "hot" to "very hot" sensations but also the transition from "cool" to "neutral" sensations. The same to the "colder" RTS.

What differs from existing thermal comfort studies mentioned in Section 1 is that the RTS proposed by us is an independent thermal sensation index, which forms a new branch of the thermal comfort theory. The 3-point RTSS sounds similar to the TP, such as the McIntyre 3-point TP scale [33] but fundamentally different. The TP accounts for the occupant's real-time thermal preference, whereas the 3-point RTSS emphasizes the occupant's real-time thermal sensation trend.

As is generally known, different materials have different thermal properties, such as specific heat capacity, heat conductivity, et cetera. Suppose there are two small particles A and B, of the same size, surrounded by the air in a steady-state thermal environment, with other physical properties being the same except for the specific heat capacity. The specific heat capacity of B is lower than that of A. When the air temperature fluctuates, on account of the different specific heat capacities, a temperature difference will be generated between A and B. When the air temperature ascends, the temperature of A will be lower than the temperature of B; when the air temperature descends, the temperature of B will be lower than the temperature of A. Therefore, it is possible to assess the air temperature trend by comparing the temperatures of A and B. As demonstrated in [34], the specific heat capacity of the skin tissues plays a vital role in protecting the deeper tissues from thermal damage, indicating that the specific heat capacity distribution of the skin tissues varies from location to location. Also, in [35], Kashcooli et al. pointed out that the skin temperature distribution is influenced by the distribution of blood vessels. Accordingly, on the human body surface, the temperatures in some areas are more easily influenced by the air temperature, while other areas may be less influenced by the air temperature due to different thermal properties on different skin or clothing locations. Also, intuitively, occupants tend to obtain a "hotter" RTS when the body surface temperature is ascending, and they tend to obtain a "colder" RTS when the body surface temperature is descending. Nevertheless, the human body is much more complicated than two particles. Based on this, we hypothesized that it is possible to use an occupant's body surface temperatures in multiple locations or their gradients to assess the RTS.

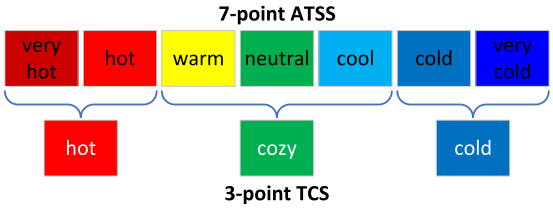

Fig. 3. 7-point Absolute Thermal Sensation Scale (7-point ATSS) and the derived 3-point Thermal Comfort Scale (3-point TCS).

2.1.2. Absolute Thermal Sensation

In order to better differentiate from the RTS, the thermal sensation in the common sense $f(t_0)$ at t_0 in Eq. (2) is denominated as the Absolute Thermal Sensation (ATS) [32]. By such a redefinition, the thermal sensation is clearly decomposed into two categories: ATS and RTS. Also, similar to the ASHRAE 7-point thermal sensation scale, we defined the 7-point Absolute Thermal Sensation Scale (7-point ATSS), as shown in Fig. 3. The 7-point ATSS has seven categories "very cold" (−3), "cold" (−2), "cool" (−1), "neutral" (0), "warm" (+1), "hot" (+2), and "very hot" (+3), each category in which is called an Absolute Thermal Sensation Vote (ATSV). Different from the ASHRAE 7-point thermal sensation scale, in the 7-point ATSS, the "cool", "neutral", and "warm" ATSVs are defined to represent comfortable sensations; the "hot" and "very hot" ATSVs are defined to represent uncomfortably hot sensations; the "cold" and "very cold" ATSVs are defined to represent uncomfortably cold sensations. Consequently, the 3-point Thermal Comfort Scale (3-point TCS), with three categories, "cold" (−3), "cozy" (0), and "hot" (+3), is derived from the 7-point ATSS. Each category in the 3-point TCS is called a Thermal Comfort Level (TCL), as illustrated in Fig. 3.

2.1.3. Composite thermal comfort model

By integrating the 3-point RTSS into the 3-point TCS (combine each TCL in the 3-point TCS with each RTS in the 3-point RTSS), the 9-point Transient Thermal Comfort Scale (9-point TTCS) is derived, which is a composite thermal comfort model and has the ability to describe both current thermal comfort and current thermal sensation trend simultaneously, as described in Fig. 4. The 9-point TTCS has nine categories "cold to cold" (−4), "cold" (−3), "cold to cozy" (−2), "cozy to cold" (−1), "cozy" (0), "cozy to hot" (+1), "hot to cozy" (+2), "hot" (+3), "hot to hot" (+4), each category in which is called a Transient Thermal Comfort Level (TTCL).

Note that in the 9-point TTCS, since the "hot", "cozy", and "cold" TTCLs are derived from the 3-point TCS and the "no change" RTS, they are also considered to be instant steady-state TCLs. The "hot to hot" and "cold to cold" TTCLs mean an occupant's hot or cold discomfort will aggravate in the future. The "hot to cozy" and "cold to cozy" TTCLs mean an occupant's hot or cold discomfort will alleviate in the future. The "cozy to hot" and "cozy to cold" TTCLs mean an occupant tends to feel uncomfortably hot or cold in the future. Even though the ATS exceeds the upper limit, the "hot to hot", "hot", and "hot to cozy" will clearly distinguish whether the hotness is aggravating or alleviating, or unchanging. The same to the lower limit of the ATS.

The 9-point TTCS makes thermal comfort modeling in the transient thermal environments clearer by explicitly using two dimensions (the RTS and TCL). If the occupant's RTS and TCL can be assessed accurately, the corresponding TTCL can be derived, which is beneficial in predicting the occupant's future TCL. For instance, suppose an occupant gets back home in winter and turns on the heater to heat the house to create a cozy environment. After turning on the heater, the occupant's current RTS will be "hotter", and the current TTCL will be "cold to cozy". After the house has been heated for some time, the occupant's TCL may transition from "cold" to "cozy". However, if the power of the heater is too high, the occupant's TTCL may finally transition to "cozy

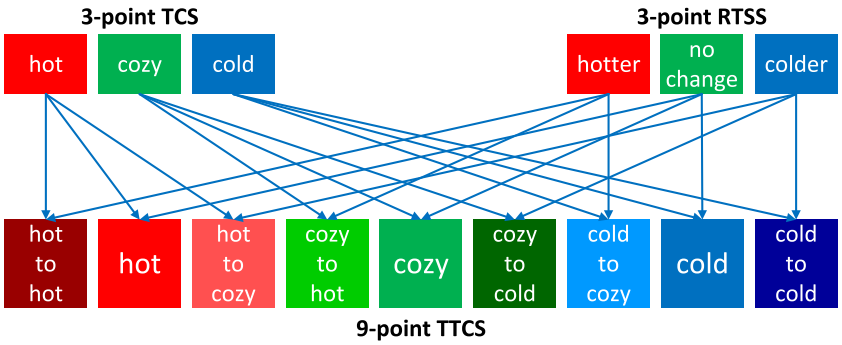

Fig. 4. 9-point Transient Thermal Comfort Scale (9-point TTCS) generated by integrating the 3-point Relative Thermal Sensation Scale (3-point RTSS) into the 3-point Thermal Comfort Scale (3-point TCS).

Fig. 5. Keyboard layout for the Absolute Thermal Sensation Vote (ATSV) and Relative Thermal Sensation Vote (RTSV) input [32].

to hot", "hot", or "hot to hot". Therefore, we can reasonably infer that the occupant's future TCL may transition from "cozy" to "hot" if the heater continues working. In that case, it would be better to turn down the power of the heater in advance to maintain the "cozy" TCL without running into the "hot" TCL. Assuming that the TTCL can be accurately assessed, not only can thermal discomfort be predicted in advance, but energy can also be saved.

2.2. Novel thermal sensation voting system

A laptop computer was utilized for the subjects' real-time ATSV and RTSV input in [32]. Fig. 5 shows the keyboard layout for the ATSV and RTSV input. The number keys "1", "2", "3", "4", "5", "6", and "7" represent the ATSVs "very cold", "cold", "cool", "neutral", "warm", "hot", "very hot", respectively. The arrow keys "up" and "down" represent the RTSVs "hotter" and "colder", respectively.

The input rule is described in Fig. 6. An alarm clock program was installed on the laptop computer to serve as a reminder for the ATSV and RTSV, ringing every 20 s. The subjects were requested to instantly input either ATSV or RTSV at least once when hearing the alarm. The priority of the ATSV is higher than that of the RTSV. Concretely, if a subject feels a distinct change in the ATS, e.g., from "warm" to "hot", the subject should press the keyboard button "6" rather than press the keyboard button "up" exclusively. On the other hand, if the latest ATSV is "warm" and the current ATSV is also "warm" while the current "warm" sensation is stronger than the latest "warm" sensation, the subject should press the "up" keyboard button to express a "hotter" RTSV. That is to say, a transition from one ATSV to another ATSV will also be counted as one RTSV input. As this study focuses on real-time thermal comfort assessment under transient thermal environments, it is necessary to gather as accurate thermal sensation as possible. Actually, instead of only inputting the ATSV and RTSV when hearing the alarm, the subjects were requested to instantly input the ATSV or RTSV whenever they felt a change in their thermal sensation.

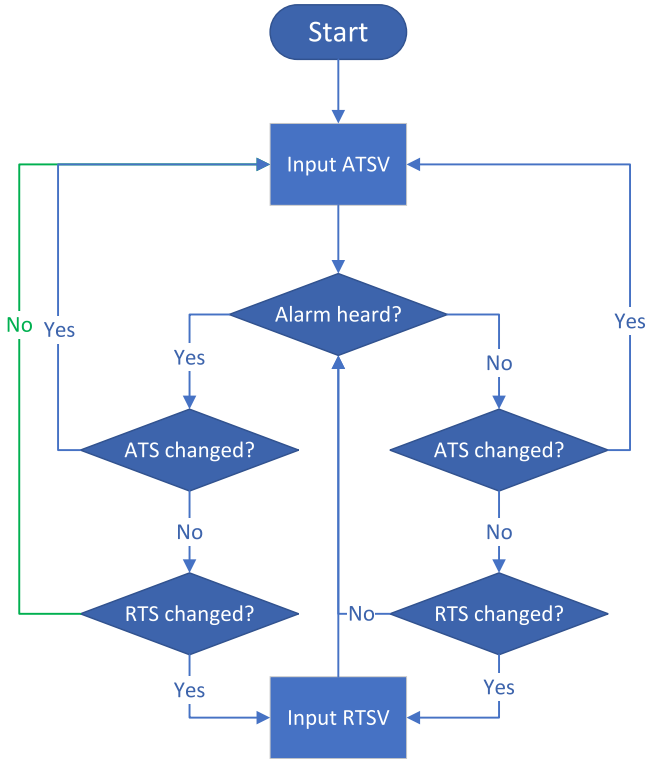

Fig. 6. Input rule of the Absolute Thermal Sensation Vote (ATSV) and the Relative Thermal Sensation Vote (RTSV).

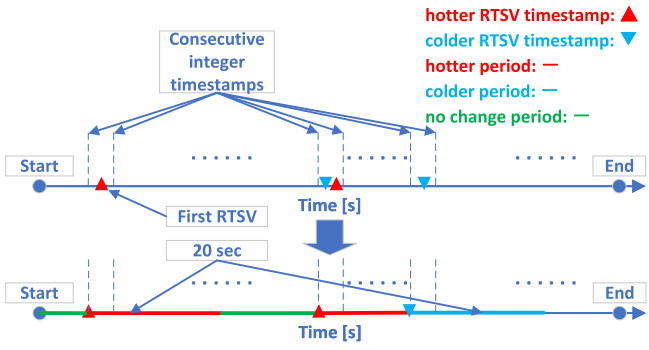

Fig. 7. Schematic of the Relative Thermal Sensation Vote (RTSV) processing method [32].

The ATSVs and RTSVs were recorded by a small keylogger program written by Python. The timestamps of the recordings of the keyboard

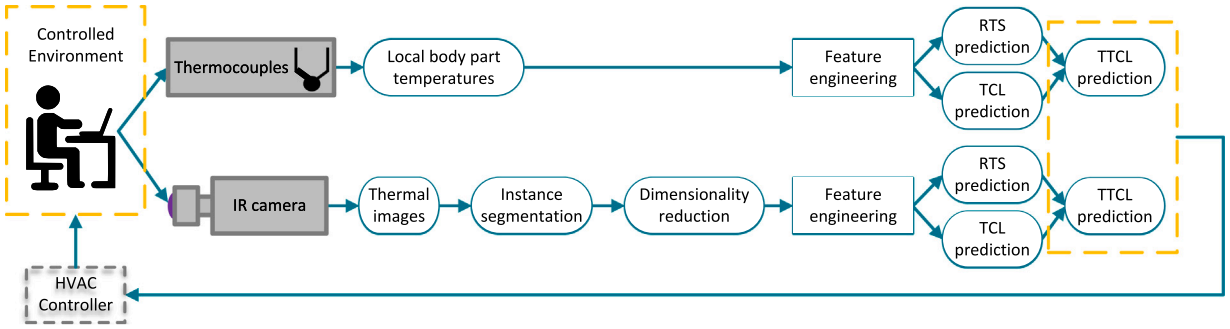

Fig. 8. Overview of the proposed intrusive and non-intrusive personal TTCL assessment framework for an occupant-centered HVAC control system.

buttons have a resolution of 0.001 s. The "hotter" and "colder" RTSVs were regarded to sustain for 20 s long (to keep consistent with the ATSV and RTSV input interval) after the input when there is no successive "hotter" or "colder" RTSV within 20 s To alleviate the subjects' mental burden, the "no change" RTSV was not set as an active vote in this study. Time periods with no "hotter" or "colder" RTS were regarded as the "no change" RTS periods.

2.2.1. RTS calculation method

The RTS calculation method is illustrated in Fig. 7. First, the resolution of the time axis of the RTS is defined as 1 s to keep consistent with the time resolution of the LBPT and the thermal images by rounding down the timestamps of the RTSVs to the nearest integers (e.g., 290.758 s → 290 s). Second, when there are multiple RTSVs within 1 s, only the last RTSV will be reserved. Third, sustained periods of the "hotter" and "colder" RTS are complemented. Finally, the "no change" periods are complemented. The time interval between the start time and the first RTSV timestamp was regarded as the "no change" period.

2.2.2. ATS and TCL calculation method

For the ATS and TCL calculation method, we also set the resolution of the time axes of the ATS and TCL to 1 s to keep consistent with the time resolution of the LBPT and the thermal images by rounding down the timestamps of the ATSVs to the nearest integers (e.g., 1151.330 s → 1151 s). When there are multiple ATSVs within 1 s, only the last ATSV will be reserved. The ATS between the start time and the first ATSV timestamp was considered the same as the first ATSV; the ATS between the last ATSV timestamp and the end time was considered the same as the last ATSV. After one ATSV input, the ATS was considered to sustain until the next ATSV input. Based on the above-mentioned rules, the subjects' whole ATS can be obtained. Next, based on Fig. 3, the subjects' TCL can be derived from the ATS.

2.3. Body surface temperature measurement

We used an intrusive method to measure the LBPT using thermocouple thermometers and a non-intrusive method using a low-cost portable infrared camera to measure the subjects' upper body thermal images.

2.3.1. Intrusive method

We measured the LBPT as illustrated in detail in [32]. We marked the locations of the ten local body parts on an anatomy human body schematic [36] which can be used for free, as shown in Fig. 9. The LBPT, as well as the air temperature, was measured by the Type *T* thermocouples (copper-constantan) per 1 s with accurate temporal synchronization and recorded by a data logger (Midi LOGGER GL840: accuracy: ±0.5 °C, resolution: 0.01 °C), as illustrated in [32].

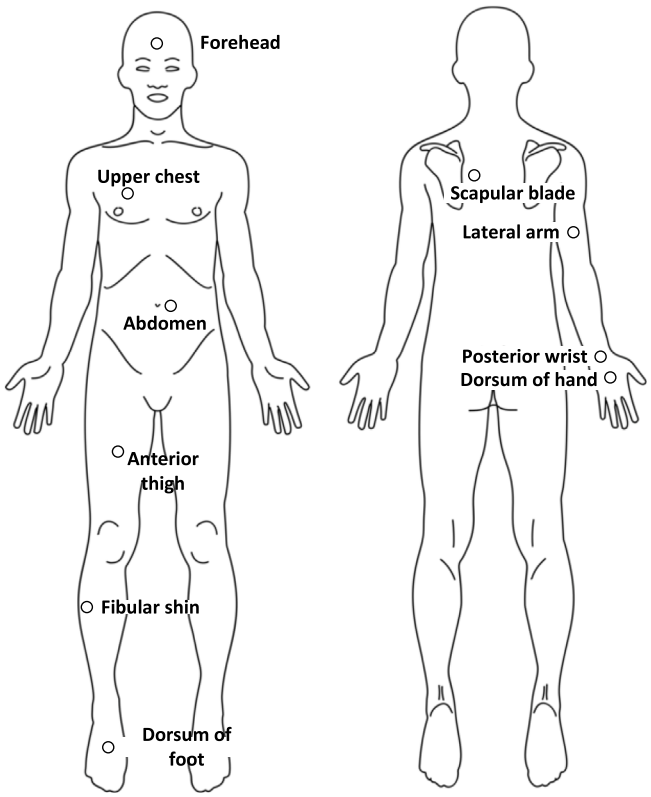

Fig. 9. Schematic of the body parts selected in this study [32].

Table 1
Specifications of the FLIR ONE Pro.

Features	Descriptions
Dimensions	6.8 cm × 1.3 cm × 4.5 cm
Weight	36 g
Resolution	120 (H) × 160 (V) pixels
Thermal sensitivity	70 mK
Accuracy	±3 °C or ±5%
Price	$375
Phone	Android (USB-C)

2.3.2. Non-intrusive method

The FLIR ONE Pro, a low-cost portable infrared camera, was used to cover infrared radiation of the subjects' upper body surface. The specifications of the FLIR ONE Pro are shown in Table 1. The FLIR ONE Pro should be connected to a smartphone to fulfill its function through the supporting app installed on the smartphone. The thermal images were taken per 1 s using the interval timer shooting mode of the device. Fig. 10 shows the mounting state of the FLIR ONE Pro. This

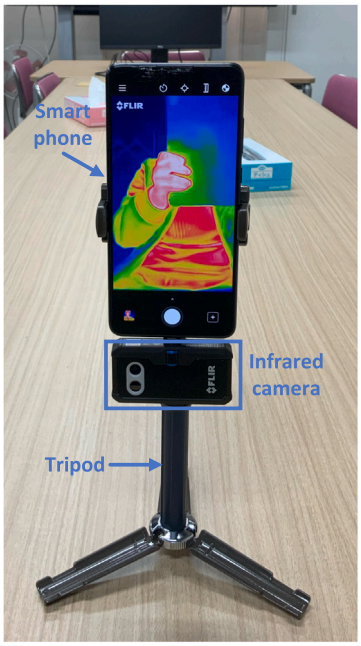

Fig. 10. Mounting state of the infrared camera (FLIR ONE Pro).

device also has a visible light photographing mode. However, we did not use this mode in this study to show the low requirement of the hardware equipment for our RTS and TCL assessment framework.

2.4. Feature extraction of thermal images

To make full use of the information in the thermal images, in this study, an instance segmentation algorithm was first used to remove the background around the person in the thermal images. Second, dimensionality reduction was applied to the segmented thermal images to perform feature extraction.

2.4.1. Thermal profile extraction

Since the background surrounding the occupant in the thermal image is unrelated to skin blood flow and thus irrelevant for thermal comfort modeling, we removed the background and extracted the subjects' thermal profiles by utilizing an instance segmentation algorithm. In [37], Bolya et al. proposed the You Only Look At CoefficienTs (YOLACT), a fully-convolutional model for real-time (> 30 fps) instance segmentation which is competitive to the state-of-the-art approaches while still running in real-time. We utilized the YOLACT++ model (the upgraded version of YOLACT by Bolya et al. in [38]) to extract the subjects' thermal profiles in the thermal images. The pre-trained weights were downloaded from the corresponding GitHub repository in [38].

2.4.2. Thermal profile dimensionality reduction

In [31], Cosma et al. demonstrated that it is possible to extract the mean temperature of each local body part as features for thermal comfort modeling, which was measured by infrared thermography. In [29], Li et al. demonstrated that it is possible to use the mean temperature of the occupants' frontal face measured by infrared thermography for thermal comfort modeling. The problem is that these kinds of mean-temperature-based methods extremely decrease the thermal information in the ROIs since an area in the thermal images has hundreds of thousands of pixels. However, since not all skin/clothing pixels in the thermal images are relevant for thermal comfort modeling, dimensionality reduction could be applied to the thermal profiles to perform feature extraction by reducing irrelevant and redundant features while preserving the most important features. According to [39], since the Principal Component Analysis (PCA) is incapable of handling non-linear data while the thermal profiles have highly non-linear features, dimensionality reduction algorithms work for non-linear data should be considered. For instance, the convolutional autoencoder (CAE), a type of artificial neural network capable of learning efficient data codings of the input data in a "self-supervised" (unsupervised) manner, which is capable of extracting spatial relationships between pixels in images [40] and widely used for dimensionality reduction. However, since the CAE consumes too much computational resource, we used the Uniform Manifold Approximation and Projection for Dimension Reduction (UMAP) [41], a general-purpose manifold learning algorithm that can be used for general non-linear dimensionality reduction while consuming less computational resource compared to the CAE. The UMAP seeks to learn the manifold structure of the data and find a low-dimensional embedding that preserves the essential topological structure of that manifold. First, the subjects' each thermal profile was flattened from the dimension 120 × 160 to a vector with a length of 19,200. Then the UMAP model was applied using the Python UMAP package with the default hyper-parameters to reduce the dimension of the flattened thermal profiles data from 19,200 to 10 to keep consistent with the LBPT. Then, the dimension-reduced thermal profiles (DRTP) were used as the extracted features of the original thermal images.

2.5. Feature engineering

Based on the knowledge that skin temperatures could be used to assess thermal comfort according to numerous studies [25–27,31], since the LBPT form an approximation of the whole body surface temperature distribution and the DRTP also form an approximation of the upper body surface temperature distribution, the LBPT and DRTP were used for TCL modeling. As the RTS is the gradient of the ATS, intuitively, we calculated and verified the gradients of the LBPT and DRTP for RTS modeling. According to Figs. 18 and 19, since the UMAP components are rather oscillative, the moving average smoothing method with a 120-s-long window size was applied to the UMAP components before calculating the gradients.

Furthermore, as mentioned in Section 2.1.1, the temperature differences between local body parts may also be relevant for RTS modeling. However, calculating the differences extremely increases the data capacity and requires more computational resources in the classification process. To account for this concern, in this study, we use the Multilayer perceptron (MLP) algorithm exclusively for classifications since the MLP classifier calculates the differences between the input variables internally, and if they are useful, the MLP classifier will use them automatically through the training process. Therefore, different from our preliminary work [32], in this study, we do not calculate differences as features to reduce redundancy and computational burden.

2.5.1. Gradients of the LBPT

The calculation method of the gradients of the LBPT is shown in Eqs. (3) and (4).

$$\overline{LT_t} = \frac{\sum_{i=-30}^{i=29} LT_{t+i}}{60} \tag{3}$$

$$LTG_t = \overline{LT_t} - \overline{LT_{t-30}} \tag{4}$$

where LT_t are the LBPT at time t; $\overline{LT_t}$ are the smoothed LBPT at time t; LTG_t are the gradient of the smoothed LBPT at time t over 30 s.

2.5.2. Gradients of the DRTP

The calculation method of the gradients of the DRTP is shown in Eqs. (5) and (6).

$$\overline{DP_t} = \frac{\sum_{i=-60}^{i=59} DP_{t+i}}{120} \tag{5}$$

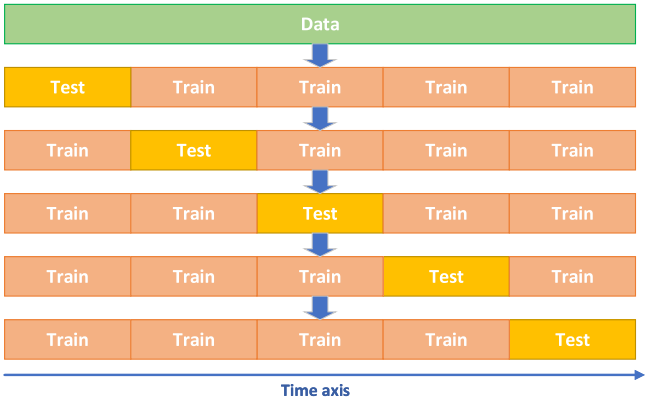

Fig. 11. Training and test set separation [32].

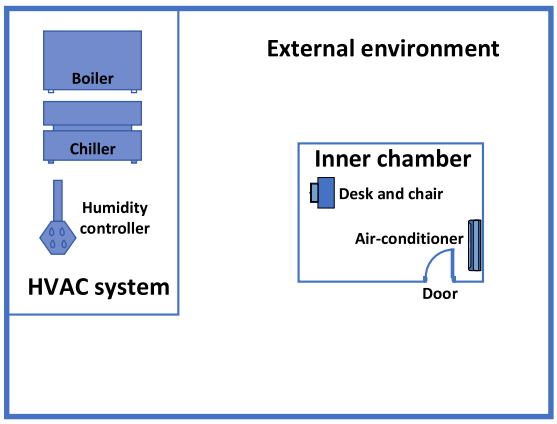

Fig. 12. Schematic of the environmental test lab [32].

$$DPG_t = \overline{DP_t} - \overline{DP_{t-30}} \tag{6}$$

where DP_t are the DRTP at time t; $\overline{DP_t}$ are the smoothed DP_t; DPG_t are the gradient of the smoothed DRTP at time t over 30 s. Since the original UMAP components are rather oscillative (see Figs. 18 and 19), a relatively long moving average window (120 s) was applied.

2.6. RTS and TCL assessments using machine learning classification algorithms

2.6.1. Feature sets of the LBPT

To analyze the validity and benefits of the extracted gradients of the LBPT for RTS and TCL assessments, three feature sets were defined as follows.

- Base feature set (Base1):
  consisted of the smoothed LBPT;
- Gradients feature set (Grad1):
  consisted of the gradients of the smoothed LBPT;
- Base and gradients feature set (BaseGrad1):
  consisted of the smoothed LBPT and the gradients of the smoothed LBPT.

2.6.2. Feature sets of the DRTP

To analyze the validity and benefits of the extracted gradients of the DRTP for RTS and TCL assessments, three feature sets were defined as follows.

- Base feature set (Base2):
  consisted of the smoothed DRTP;
- Gradients feature set (Grad2):
  consisted of the gradients of the smoothed DRTP;
- Base and gradients feature set (BaseGrad2):
  consisted of the smoothed DRTP and the gradients of the smoothed DRTP.

2.6.3. Classification algorithm

We used the MLP classifier to assess the validity of each feature set defined in Sections 2.6.1 and 2.6.2 to predict personal RTS and TCL. The MLP classifier was trained using the Python Scikit-learn package. Optimal hyper-parameters of the MLP classifier were obtained using the grid search technique (i.e., 'hidden_layer_sizes': [(10,), (20,), (30,), (40,), (50,), (60,), (70,), (80,)], 'max_iter'=200, 'activation': ['tanh', 'relu'], 'solver': ['sgd', 'adam'], 'alpha': [0.0001, 0.05], 'learning_rate': ['constant', 'adaptive']).

2.6.4. Personal RTS and TCL assessments

The feature sets defined in Sections 2.6.1 and 2.6.2 were used as the training data after normalization, and the RTS and TCL derived from the subjects' RTSVs and ATSVs according to Sections 2.2.1 and 2.2.2 were used as labels for personal RTS and TCL classifications. Owing to the limited data capacity, in order to make full use of the data, we carried out the 5-fold blocked cross-validation without shuffling suggested by [42,43] since the data have time dependencies, in which each subject's data samples were segmented into five equal-sized parts according to chronological order, as illustrated in Fig. 11. Next, by iterating the process of using four parts as the training set and using the remaining one part as the test set, each part will be used as the test set once and generates the prediction. By merging all the predictions generated by all the test sets, the whole prediction can be generated. Then, the TTCL prediction can be derived by integrating the RTS prediction into the TCL prediction according to Fig. 4.

3. Experimental setup

We conducted the experiment in the winter season (February 2020) at the environmental test lab of Tokyo Gas Co., Ltd, which consists of an HVAC system, an external environment, and an inner chamber, as illustrated in Fig. 12. The HVAC system is equipped with a boiler, a chiller, and a humidity controller, which is used to control the air temperature and relative humidity of the external environment. There is an air-conditioner installed in the inner chamber to adjust the air temperature inside the inner chamber. When turning on the air-conditioner, the air temperature in the inner chamber (T_I) can be gradually adjusted. Additionally, the inner chamber has a door to allow ventilation through the external environment. Since the volume of the external environment is much larger than the volume of the inner chamber, the air temperature in the external environment (T_E) can be regarded as changeless when opening the door to make heat exchange, and T_I will change very fast. Consequently, T_I will be drastically adjusted to T_E approximately. We utilized this property to simulate a rapid temperature-changing phase in the inner chamber.

3.1. Thermal conditions

T_E and the relative humidity in the external environment were set to 18 °C and 50% throughout the experiment. Instead of steady-state thermal environments, transient thermal environments were simulated in this study by creating a series of cooling and heating phases in the inner chamber by operating the HVAC system, the air-conditioner, and the door. The door was kept open to keep the thermal condition of the inner chamber approximately equal to the thermal condition of the external environment before the experiment. Two temperature-changing scenarios were created, as illustrated in the following Sections.

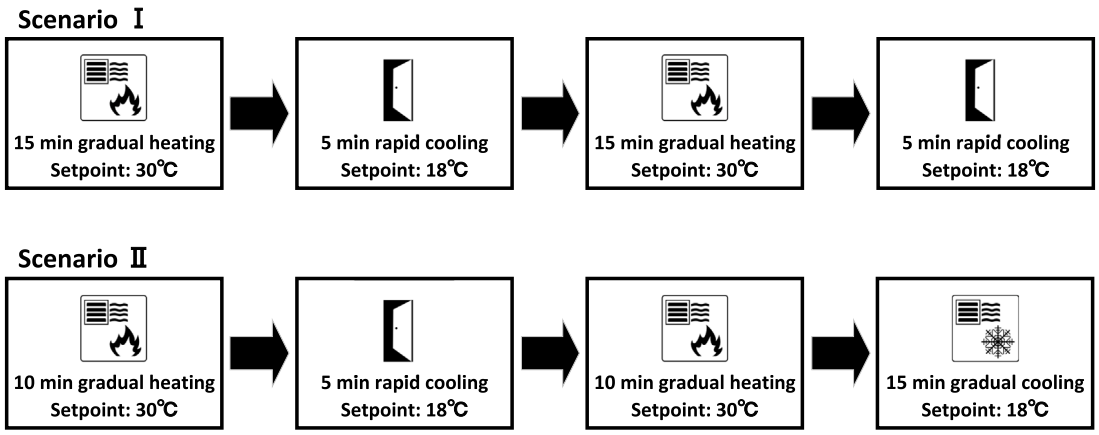

Fig. 13. Temperature scenarios in the inner chamber [32].

3.1.1. Scenario I

The temperature control scheme of Scenario I is described in the upper part of Fig. 13. First, close the door and turn on the air-conditioner to gradually heat the inner chamber for 15 min, and the setpoint was set to 30 °C. The 15-min-long heating phase is long enough to sufficiently heat the inner chamber to make T_I level off during the latter half of the heating phase. The second phase was a rapid cooling phase by turning off the air-conditioner and opening the door for 5 min. The latter two phases were identical to the former two phases. By repeating the above-mentioned two phases, a periodic temperature signal with a period of 20 min can be generated. The total duration of Scenario I was 40 min. Scenario I was simulated to investigate the RTS behaviors when T_I starts to level off after being sufficiently heated or cooled in the heating and cooling phases.

3.1.2. Scenario II

The temperature control scheme of Scenario II is described in the lower part of Fig. 13. Similar with Scenario I, two identical gradual heating phases were simulated by closing the door and turning on the air-conditioner to heat the inner chamber, and the setpoint was set to 30 °C. The first cooling phase is the same as the rapid cooling phase in Scenario I. Different from Scenario I, a gradual cooling phase was applied in Scenario II to replace the second rapid cooling phase in Scenario I, in which the door was closed, and the setpoint of the air-conditioner was set to 18 °C to keep consistent with T_E. The gradual cooling phase was set to 15 min long enough to ensure T_I to be lowered approximately to 18 °C by the end of the cooling phase. Additionally, either of the two heating phases was shortened to 10 min to keep the total experiment duration to 40 min to keep consistent with Scenario I. Scenario II was simulated to observe the RTS behaviors under completely two different cooling phases.

3.2. Experimental procedure

Six subjects participated in the experiment. All of them are male students (age 25 ± 1 years) at the University of Tokyo. Three students were randomly chosen and dispatched to Scenario I, and the other three were dispatched to Scenario II.

A desk and a chair were prepared in the inner chamber. The laptop computer for the ATSV and RTSV input was placed on the desk. The desk and chair were positioned not to directly face the airflow from the door or the air-conditioner, as illustrated in Fig. 12. During the experiment, sedentary office activities were simulated by letting the subjects sit down on the chair and press the keyboard buttons to input the ATSV and RTSV (small range of motions allowed). Also, the same clothes (black short sleeves, trousers, and cotton socks) were provided to the subjects during the experiment. The subjects were requested not

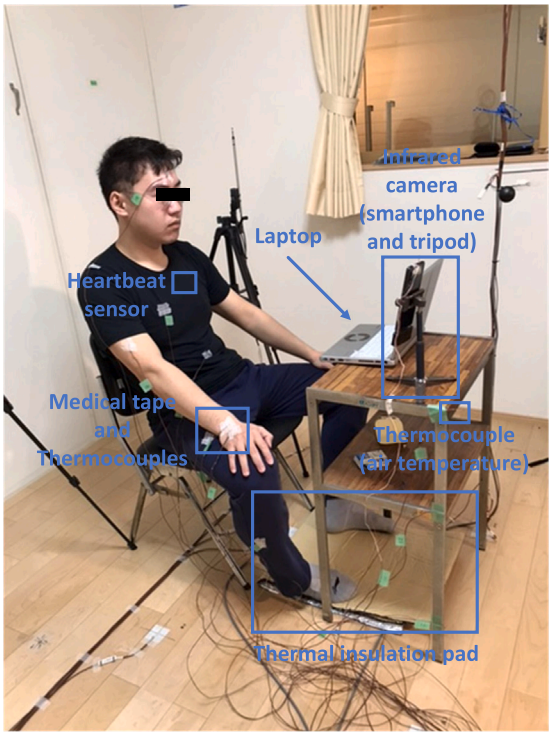

Fig. 14. The mounting state of the experimental devices on a male subject.

to perform large motions and put their hands on their thighs when not pressing the keyboard. A thermal insulation pad was put under the desk on the floor to prevent unnecessary conductive heat loss from the subjects' feet to the floor. The subjects were confirmed whether their current RTS is "no change" or not for preparation before the experiment to maintain a steady-state thermal sensation.

During the preparation time (20 min), we fixed the thermocouples onto the subjects' specific local body parts as illustrated in Fig. 9 using medical tapes. At the forehead, the lateral arm, the posterior wrist, the dorsum of the hand, skin temperatures were measured. In contrast, at the upper chest, the abdomen, the scapular blade, the anterior thigh, the fibular shin, the dorsum of the foot, clothing temperatures were measured. The subjects were requested to use the left hand to press the keyboard to input the real-time RTSV and ATSV since the right hand was adhered with thermocouples by the medical tape to measure the skin temperatures. In addition, we also fixed a portable heartbeat sensor onto the subject's chest to measure the heartbeat data

Table 2
Statistics of the number of original RTSVs and ATSVs by each subject.

Scenario	Subject ID	RTSV		ATSV	Total
		Hotter	Colder		
I	1	62	41	73	176
	2	66	128	118	312
	3	56	47	76	179
II	4	41	55	175	271
	5	65	67	139	271
	6	51	45	84	180

Table 3
Total duration (s) of each subject's each RTS category.

Scenario	Subject ID	RTS		
		Hotter	No change	Colder
I	1	1060	813	527
	2	884	863	653
	3	838	829	733
II	4	890	866	644
	5	1143	721	536
	6	866	846	688

for thermal comfort modeling trials, as shown in Fig. 14. The results were promising but beyond the scope of this paper.

The infrared camera was connected to a smartphone, and the smartphone was placed on a tripod to uphold it to make the visual field of the infrared camera controllable to cover the upper body (except for the hands and a portion of the lower arms) of the subject since in actual sedentary office activities the lower limbs are always occluded by the desk if the infrared camera is placed on the desk. The angle and position of the infrared camera were adjusted optimally for each subject and kept constant throughout the experiment. In addition, since placing the infrared camera directly opposite the subject increases the requirement of the framework, and sometimes this could be disturbing to the subjects, we put the infrared camera on the right front side of the desk at a small angle from the direct front of the subject to verify the superiority of our method over the ROI-extraction-based methods as mentioned in Section 1.

Fig. 14 shows a male subject and the mounting state of the experimental devices. The ambient air temperature was measured by a pair of thermocouples placed 60 cm above the floor near the subject, as shown in Fig. 14. The subjects were not aware of the opening and closing of the door and the operations of the air-conditioner, and were requested to input the ATSV and RTSV according to subjective thermal feelings. The Research Ethics Committee of the University of Tokyo approved the experiment.

4. Results and discussion

The statistics of the number of original RTSVs and ATSVs by each subject are summarized in Table 2. Suppose a subject inputs at least once per 20 s, the total number of the RTSVs and ATSVs should be at least 120, and all the subjects input more than 120 times throughout the experiment, as shown in Table 2. Table 3 summarizes the total duration of each RTS category of each subject. It can be observed that the class imbalance is not severe, and each RTS category takes a relatively balanced duration for all subjects.

4.1. Data visualization

Fig. 15(a) shows an original thermal image of a subject. Fig. 15(b) shows the instance segmentation example of Fig. 15(a) using the YOLACT++ model as illustrated in Section 2.4.1. It can be observed that the model works very well in extracting the subject's thermal profile from the thermal image even though the model was trained on a visible image dataset.

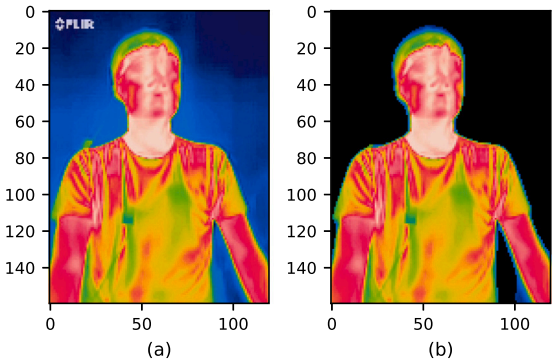

Fig. 15. An example of the instance segmentation result ((a): original thermal image, (b): segmented thermal image).

The boxplot (Fig. 16) shows the four quartile distribution of each subject's LBPT. In both Scenarios I and II, common features exist, such that the clothing temperatures have a relatively wider range (the length of the rectangle) than that measured on the skin since the clothing has a lower specific heat capacity than the skin. Thus its temperature is more easily influenced by the ambient air temperature. Moreover, the forehead temperature reached the highest range among all the local body parts. Though noticeable individual differences among the subjects can be observed, no obvious difference can be observed between Scenarios I and II.

The boxplot (Fig. 17) shows the four quartile distribution of each subject's DRTP. In both Scenarios I and II, common features can be observed such that the first half of the UMAP components have a relatively wider range (the length of the rectangle) than the latter half of the UMAP components roughly. Though noticeable individual differences among the subjects can be observed, no obvious difference can be observed between Scenarios I and II.

Figs. 18 and 19 show the representative data of two subjects from Scenarios I and II, respectively. The air temperature is drawn in the black line; the shin and abdomen temperatures are drawn in light blue and orange lines, respectively; the original "hotter" and "colder" RTSVs are drawn in red and blue triangles, respectively; the original ATSVs are drawn in black circles; the first two UMAP components are drawn in cyan and violet lines, respectively. In addition, the smoothed two UMAP components are drawn in green and dark blue lines, respectively.

In both Figs. 18 and 19, we can observe that the UMAP components are rather oscillative since the original accuracy of the infrared camera is not high (see Table 1), and the moving average method is very effective in removing the noise in the UMAP components.

In both Figs. 18 and 19, "hotter" RTSVs mostly appear in the heating phases, and "colder" RTSVs mostly appear in the cooling phases. In Fig. 18, in the latter half of the first heating phase, the air temperature leveled off, and the "hotter" RTSVs became fewer during this period; in the first cooling phase, the air temperature abruptly dropped due to the effect of opening the door and leveled off rapidly, and the "colder" RTSVs became fewer during the latter half of this phase. In Fig. 19, during the first cooling phase, the air temperature abruptly dropped due to the effect of opening the door. However, the air temperature had a small increment after the abrupt drop. Interestingly, even though the air temperature ascended a little, the subject still densely gave "colder" RTSVs during this period, indicating that the RTS does not always follow the current air temperature trend but can also be influenced by the previous context.

As can be observed in both Figs. 18 and 19, the air temperature during both first rapid cooling phases was no higher than that at the beginning of the experiment. However, the two subjects's ATS in the

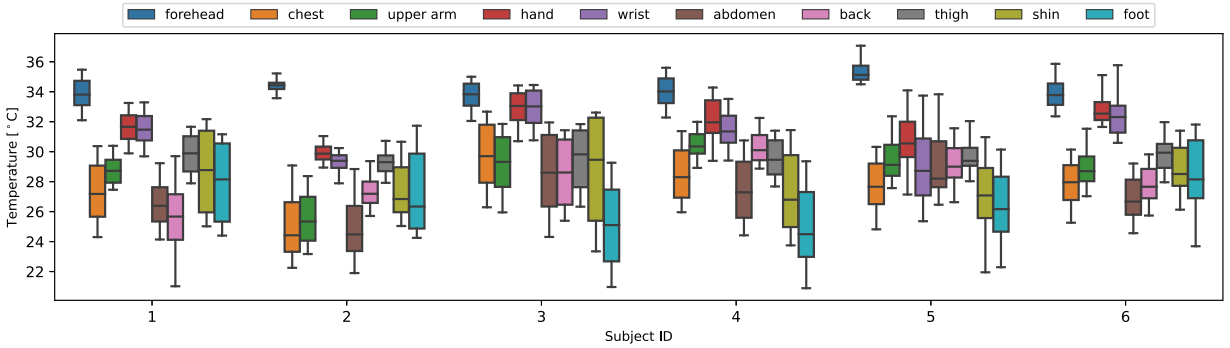

Fig. 16. Boxplot of the LBPT for all subjects (Scenario I: subject 1–3, Scenario II: subject 4–6) [32].

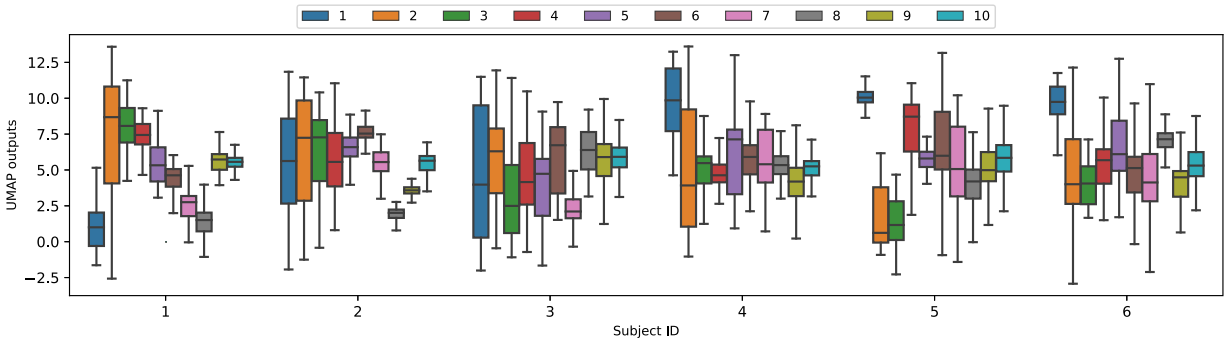

Fig. 17. Boxplot of the DRTP for all subjects (Scenario I: subject 1–3, Scenario II: subject 4–6).

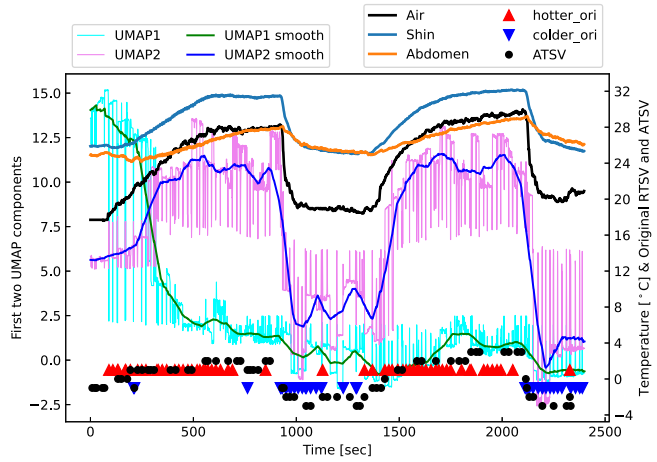

Fig. 18. Air temperature, shin and abdomen temperatures, original ATSVs and RTSVs, first two UMAP components, and smoothed first two UMAP components (Scenario I & subject 1).

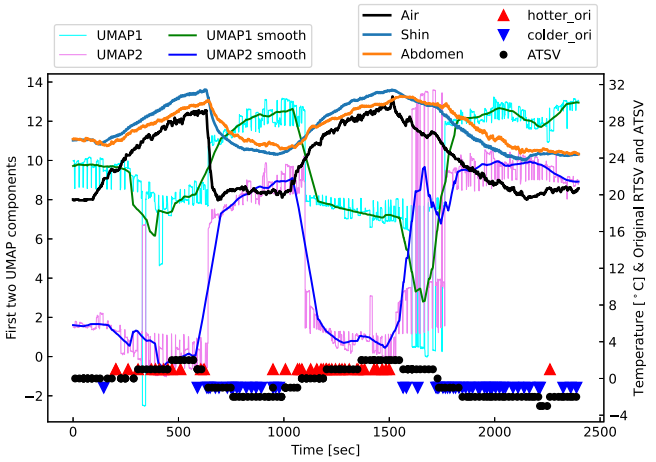

Fig. 19. Air temperature, shin and abdomen temperatures, original ATSVs and RTSVs, first two UMAP components, and smoothed first two UMAP components (Scenario II & subject 4).

first rapid cooling phase is colder than that at the beginning of the experiment, indicating that the ATS is not monotonically determined by the current air temperature but can also be influenced by the previous context.

In both Figs. 18 and 19, for the LBPT, we can observe that the ATSVs are positively and strongly correlated with the shin and abdomen temperatures. For the DRTP, in Fig. 19, both of the first two smoothed UMAP components strongly correlate with the ATSVs negatively. However, what is noticeable is that different from the LBPT, in Fig. 18, only the second smoothed UMAP component shows a strong positive correlation with the ATSVs while the first smoothed UMAP component does not since the UMAP is a non-linear process and the transformation does not preserve physical meanings. The obvious positive or negative correlations between the LBPT as well as a portion of the DRTP and the ATS indicate that the LBPT and DRTP could be reasonable for ATS modeling.

In Scenario I, identical heating and cooling phases appeared in pairs, whereas in Scenario II, the two cooling phases were completely different. Nonetheless, in both Figs. 18 and 19, during "hotter" periods, the shin temperature is higher than the abdomen temperature, whereas during "colder" periods, the abdomen temperature is higher than the shin temperature, which agrees with our hypothesis mentioned in Section 2.1.1, indicating that it could be reasonable to use the LBPT for RTS modeling in both Scenarios I and II. In both Figs. 18 and 19, during "hotter" periods, the shin and abdomen temperatures are ascending, whereas during "colder" periods, they are descending, indicating that it

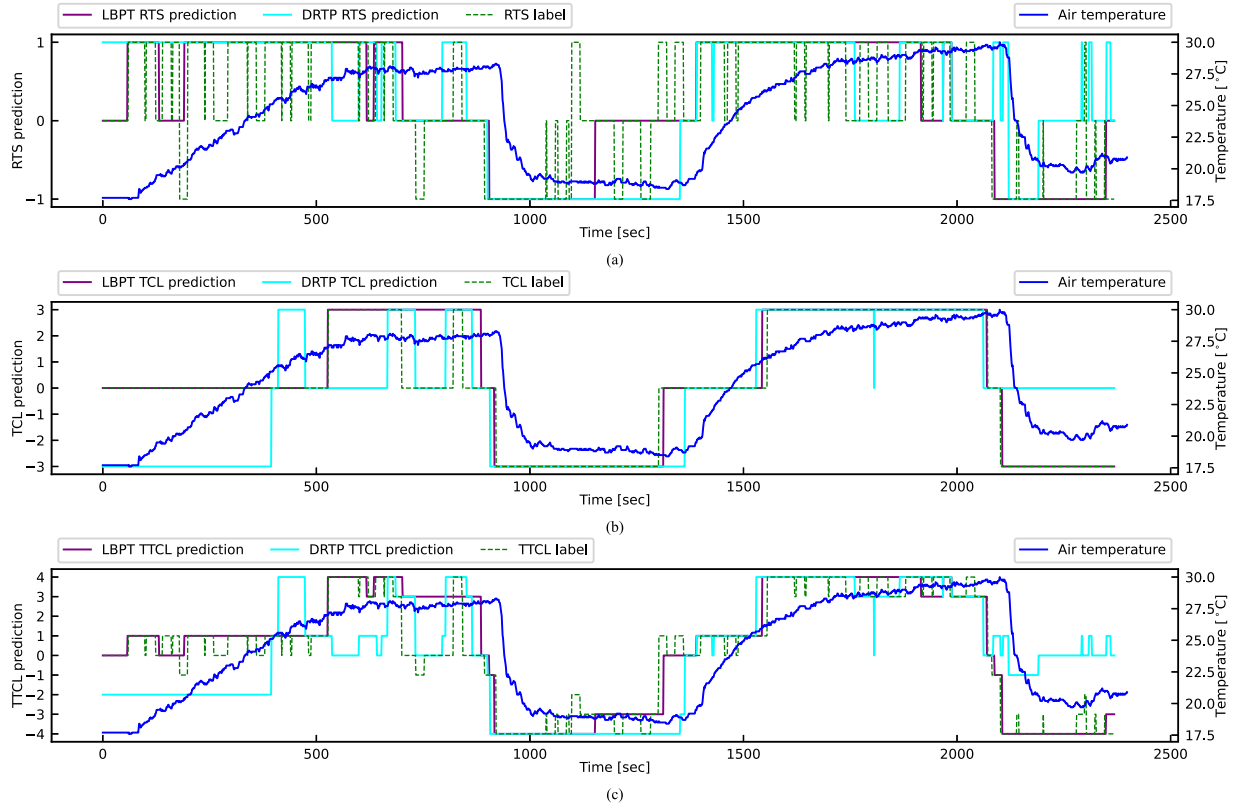

Fig. 20. Predictions of the RTS (Grad1 and BaseGrad2 feature sets), predictions of the TCL (Base1 and Base2 feature sets), and the integrated TTCL predictions (Scenario I & Subject 1).

Table 4
Mean accuracy (unit: %) of the RTS and TCL classifications in Scenarios I and II for all feature sets.

RTS or TCL	Scenario	LBPT feature sets			DRTP feature sets		
		Base1	Grad1	BaseGrad1	Base2	Grad2	BaseGrad2
RTS	I	64.1	67.2	66.5	55.8	51.3	58.6
	II	59.6	62.9	62.7	52.6	48.1	56.1
TCL	I	86.8	77.8	87.5	70.5	55.7	74.3
	II	80.3	63.9	78.2	73.4	55.4	67.8

could be reasonable to use the gradients of the LBPT for RTS modeling. For the DRTP, since the UMAP components do not preserve physical meanings, calculating differences between UMAP components makes nonsense. What is noticeable is that, in Fig. 18, for the second smoothed UMAP component, during "hotter" periods, it occupies a higher range, while during "colder" periods, it occupies a lower range; in Fig. 19, for both smoothed UMAP components, during "hotter" periods, they occupy lower ranges; during "colder" periods, they occupy higher ranges, indicating that it could be reasonable to use the DRTP for RTS modeling.

4.2. TCL, RTS and TTCL assessments

Table 4 shows the mean accuracy of the RTS and TCL predictions in Scenarios I and II using the LBPT or DRTP feature sets, respectively. Table 5 shows the mean precision and recall of the RTS and TCL classifications using the LBPT feature sets and the DRTP feature sets, respectively. Figs. 20 and 21 show the RTS predictions, TCL predictions, and the integrated TTCL predictions using the LBPT or DRTP feature sets of the two subjects from Scenarios I and II, respectively, as we mentioned before. In Figs. 20 and 21, for the RTS assessment, the Grad1 and BaseGrad2 feature sets were used; for the TCL assessment, the Base1 and Base2 feature sets were used.

4.2.1. TCL assessment

As can be observed in Table 4, for the TCL predictions using the LBPT feature sets, the Base1 feature set reached a mean accuracy of more than 80% in both Scenarios I and II, indicating that the LBPT are relevant for TCL modeling, which has been demonstrated by numerous studies. The Grad1 feature set reached a mean accuracy of 77.8% and 63.9% in Scenarios I and II, respectively, which is lower than the accuracy obtained by the Base1 feature set but still not bad, indicating that the gradients of the LBPT are also relevant for TCL modeling, which is similar with the conclusions that skin temperature gradient can also be relevant for thermal comfort modeling as demonstrated in some studies [5,31,44]. However, by adding the Base1 and Grad1 feature sets together, the BaseGrad1 feature set performed better than the Base1 feature set in Scenario I while a little worse in Scenario II. The reason is considered to be the lack of sufficient training data, and an accuracy of approximately 80% might be the limit of the predictability of the TCL.

For the TCL predictions using the DRTP feature sets, the Base2 feature set reached a mean accuracy of more than 70% in both Scenarios I and II, indicating that the DRTP are relevant for TCL modeling. The Grad2 feature set reached a mean accuracy of 55.7% and 55.4% in Scenarios I and II, respectively, which is significantly lower than the accuracy obtained by the Base2 feature set. Also, the BaseGrad2 feature set outperformed the Base2 feature set in Scenario I but underperformed in Scenario II, indicating that the gradients of the DRTP are less relevant or irrelevant for TCL modeling.

As can be observed in Table 5, for the TCL classifications using the Base1, Grad1, and BaseGrad1 feature sets, by combining the Base1 and Grad1 feature sets together, the BaseGrad1 feature set obtained a more balanced precision and recall (i.e., no precision and recall lower than 70.1%) for all TCL categories in Scenarios I and II, indicating that both Base1 and Grad1 feature sets are relevant for TCL modeling, which agrees with the conclusion we mentioned above.

Table 5
Mean precision and recall (unit: %) of the RTS and TCL classifications in Scenarios I and II for all feature sets (P: precision, R: recall).

Category	Scenario	LBPT feature sets						DRTP feature sets					
		Base1		Grad1		BaseGrad1		Base2		Grad2		BaseGrad2	
		P	R	P	R	P	R	P	R	P	R	P	R
RTS-hotter	I	74.6	73.4	75.9	75.5	76.8	77.5	60.3	52.2	59.2	55.3	64.5	57.0
RTS-no change	I	36.2	33.5	45.4	33.2	52.6	40.3	44.5	36.0	37.5	37.1	42.3	39.5
RTS-colder	I	64.4	80.8	68.1	86.5	67.1	78.3	61.4	75.1	57.6	57.0	65.4	74.9
RTS-hotter	II	59.6	65.9	65.1	71.3	69.4	71.7	54.9	49.5	58.6	47.4	71.3	51.7
RTS-no change	II	54.9	48.6	57.2	48.8	53.8	47.7	57.7	59.5	44.1	52.9	50.5	60.6
RTS-colder	II	64.7	68.3	67.2	74.2	67.9	72.6	45.1	43.8	48.9	40.9	56.8	48.3
TCL-hot	I	91.6	94.9	87.7	86.1	98.3	89.6	76.0	61.0	49.5	56.5	91.0	73.1
TCL-cozy	I	85.7	79.6	71.4	77.2	84.8	84.6	66.7	64.2	54.2	51.6	66.3	73.0
TCL-cold	I	83.5	90.3	76.6	69.8	84.8	91.0	69.2	81.8	54.5	49.7	71.3	72.0
TCL-hot	II	81.0	79.0	52.7	54.9	70.1	73.4	74.1	56.8	71.8	32.8	68.4	56.9
TCL-cozy	II	82.3	81.4	65.9	64.8	80.9	78.4	77.9	77.9	62.0	71.7	71.9	69.1
TCL-cold	II	52.4	58.3	48.9	38.2	76.8	80.0	62.3	84.1	23.3	28.7	71.9	64.6

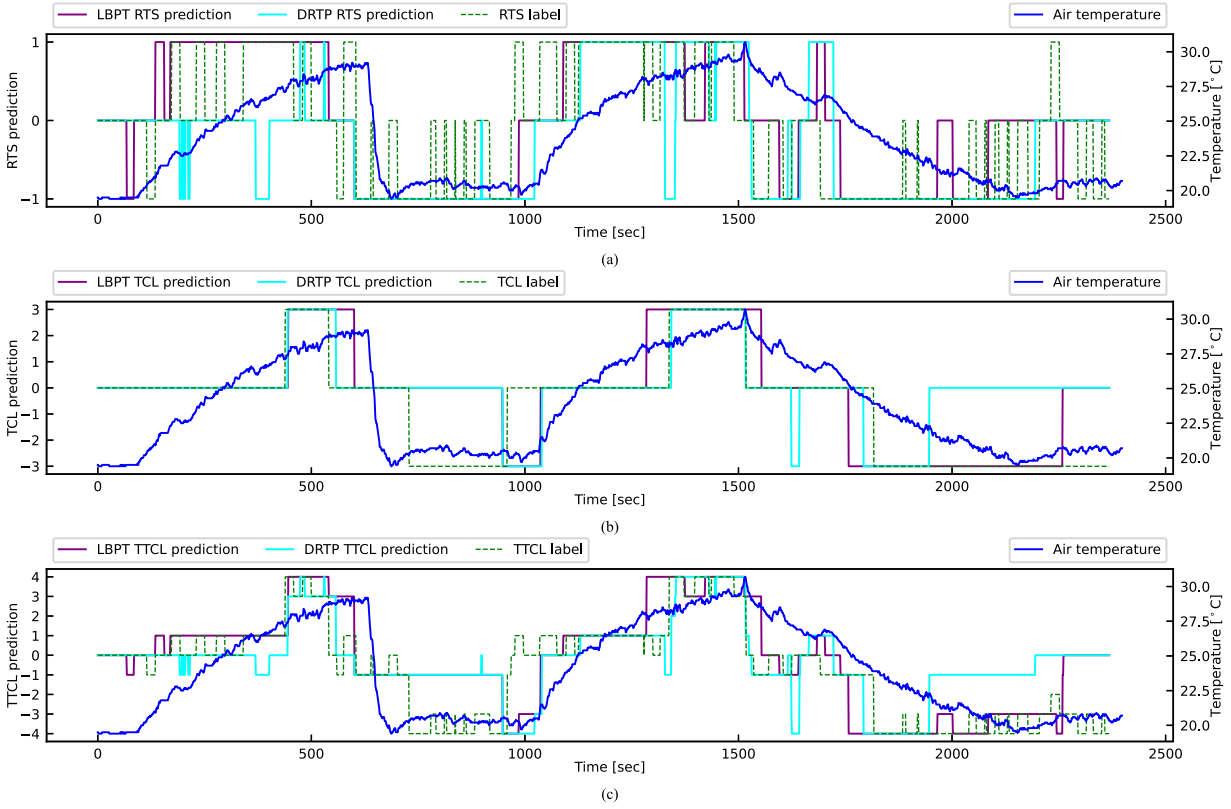

Fig. 21. Predictions of the RTS (Grad1 and BaseGrad2 feature sets), predictions of the TCL (Base1 and Base2 feature sets), and the integrated TTCL predictions (Scenario II & Subject 4).

For the TCL predictions in Figs. 20 and 21, the Base1 and Base2 feature sets performed fairly well in predicting the general trends of the TCL. Moreover, since the Base1 feature set performed better than the Base2 feature set in both Scenarios I and II, the intrusive method outperformed the non-intrusive method in the TCL assessment.

4.2.2. RTS assessment

As can be observed in Table 4, for the RTS predictions using the LBPT feature sets, the Grad1 feature set performed better than the Base1 feature set in both Scenarios I and II and reached a mean accuracy of 67.2% and 62.9% in Scenarios I and II, respectively. Compared to the TCL assessment, the Grad1 feature set has a much stronger impact on the RTS assessment.

The overall RTS prediction accuracy is significantly lower than the TCL prediction accuracy for all feature sets, as shown in Table 4. The reason is considered to be that the limit of the predictability of the RTS is fundamentally lower than the TCL since the RTS has much more fine details (i.e., the frequent intermittent "no change" RTS) than the TCL, as shown in Figs. 20 and 21. Therefore, an accuracy of 60%–70% might be the limit of the predictability of the RTS. From this point of view, both Base1 and Grad1 feature sets performed fairly well in both Scenarios I and II, indicating that the LBPT and the gradients of the LBPT are both relevant for RTS modeling which agrees with our hypothesis proposed in Section 2.1.1. Also, it is noticeable that the BaseGrad1 feature set reached a little lower accuracy than the Grad1 feature set. The reason is considered to be the lack of sufficient training data.

For the RTS predictions using the DRTP feature sets, the Base2 feature set reached a mean accuracy of 55.8% and 52.6% in Scenarios I and II, respectively. On the other hand, the Grad2 feature set reached a mean accuracy of 51.3% and 48.1% in Scenarios I and II, respectively,

Table 6
Mean accuracy (unit: %) of the TTCL predictions in Scenarios I and II using LBPT features (RTS: Grad1, TCL: Base1) or DRTP features (RTS: BaseGrad2, TCL: Base2).

	Scenario	LBPT	DRTP
TTCL	I	59.7	45.3
	II	52.0	42.7

which has a relatively similar performance to the Base2 feature set. Compared to the TCL assessment, the Grad2 feature set has a relatively stronger impact on the RTS assessment. By combining the Base2 and Grad2 feature sets together, the RTS prediction accuracy considerably increased using the BaseGrad2 feature set, which performed best in both Scenarios I and II and reached a mean accuracy of 58.6% and 56.1%, respectively. Therefore, it is concluded that the DRTP and the gradients of the DRTP are both relevant for RTS modeling, which agrees with our hypothesis proposed in Section 2.1.1.

Since the RTS has many frequent intermittent "no change" periods, it is conceivable that it is more difficult to predict the "no change" RTS than the "hotter" or "colder" RTS. Therefore, as can be observed in Table 5, for the RTS classifications by all feature sets, the "no change" RTS obtained a relatively lower precision and recall than the "hotter" and "colder" RTS. Furthermore, by combining the Base1 and Grad1 feature sets together, the BaseGrad1 feature set obtained a more balanced precision and recall than the Base1 and Grad1 feature sets (i.e., no precision and recall lower than 40.3%) for all RTS categories in Scenarios I and II, indicating that both Base1 and Grad1 feature sets are relevant for RTS modeling, which agrees with the conclusion we mentioned above. For the RTS classifications using the Base2, Grad2, and BaseGrad2 feature sets, by combining the Base2 and Grad2 feature sets together, the BaseGrad2 feature set obtained a more balanced precision and recall (i.e., no precision and recall lower than 39.5%) for all RTS categories in Scenarios I and II, indicating that both Base2 and Grad2 feature sets are relevant for RTS modeling, which agrees with the conclusion we mentioned above.

As can be observed in Fig. 20, in the former half of the two gradual heating phases, the air temperature gradually increased, and the subject's RTS was "hotter" mainly. However, many short periods of "no change" RTS can be observed in the two gradual heating phases even when the air temperature was continuously increasing. In Fig. 21, in the rapid cooling phase, the air temperature did not monotonously go down after opening the door but got an increment after the abrupt drop. It is remarkable that the subject had no "hotter" RTS but still continuously got "colder" RTS mainly during this period, indicating the context-dependent property of the RTS as we illustrated above. If the RTS were simply assessed by observing the ambient air temperature, mistakes would be made.

In Figs. 20 and 21, the RTS trend was successfully predicted using both LBPT and DRTP feature sets, especially in the latter half of the first gradual heating phase in Fig. 20 and the latter half of the gradual cooling phase in Fig. 21, when the air temperature leveled off, the "no change" RTS was well predicted using both LBPT and DRTP feature sets.

Moreover, since the Grad1 feature set performed better than the BaseGrad2 feature set in both Scenarios I and II as shown in Table 4, the intrusive method outperformed the non-intrusive method in the RTS assessment. For example, in Fig. 20, in the latter half of the first cooling phase when the air temperature leveled off, the subject's RTS became "no change" and was only well predicted by the Grad1 feature set.

4.2.3. TTCL assessment

Table 6 shows the mean accuracy of the TTCL predictions in Scenarios I and II integrated by the RTS predictions and the TCL predictions using the LBPT features (RTS: Grad1, TCL: Base1) or DRTP features (RTS: BaseGrad2, TCL: Base2). The LBPT features reached a mean accuracy of 59.7% and 52.0% in Scenarios I and II, respectively; the DRTP features reached a mean accuracy of 45.3% and 42.7% in Scenarios I and II, respectively. Therefore, the intrusive method outperformed the non-intrusive method. The prediction result is not bad as the number of classes of the TTCL is relatively large (nine). The TTCL prediction accuracy obtained in this paper using the LBPT features is much higher than that in our preliminary work [32], and also higher than that in the conference paper [45].

The significance of the 9-point TTCS is that "cozy to hot" and "cozy to cold" TTCLs can generate thermal discomfort early warning mechanisms from running into "hot" or "cold" TCLs. For instance, in Fig. 20, in the second gradual heating phase, during 1400–1550 s, the subject's RTS was "hotter" while the TCL was still "cozy" after turning on the heating mode of the air-conditioner, the TTCL was mostly "cozy to hot" and was successfully predicted by both LBPT and DRTP features; in Fig. 21, in the rapid cooling phase, during 600–700 s, the subject's RTS was "colder" while the TCL was still "cozy" after turning on the cooling mode of the air-conditioner, the TTCL was mostly "cozy to cold" and was successfully predicted by both LBPT and DRTP features.

Moreover, the significance of the 9-point TTCS is that "hot to hot" and "cold to cold" TTCLs can generate thermal discomfort deterioration prevention mechanisms that can prevent current thermal discomfort from deteriorating. For instance, in Fig. 20, in the second gradual heating phase, during 1550–1800 s, the subject's RTS was "hotter" while the TCL was "hot", the TTCL was mostly "hot to hot" and was successfully predicted by both LBPT and DRTP features; in Fig. 21, in the gradual cooling phase, during 1800–1950 s, the subject's RTS was "colder" while the TCL was "cold", the TTCL was mostly "cold to cold" and was successfully predicted by both LBPT and DRTP features.

4.3. Limitations

The limitations of this study are illustrated as follows. Firstly, considering the subjects' mental burden, the "no change" RTSV was not set to an active vote, and the duration of the "hotter" and "colder" RTSVs was regarded to sustain for 20 s. However, a rather slight "hotter" or "colder" RTSV may not sustain for 20 s, resulting in possible inaccurate RTS acquisitions.

Secondly, since the 3-point TCS is derived from the 7-point ATSS, three categories of the ATS ("warm", "neutral", and "cool") are integrated to one "cozy" TCL. Therefore, the "cozy to hot" and "cozy to cold" TTCLs may not mean the TCLs are deviating from "cozy" and cause ambiguities. For example, suppose an occupant's original ATS is transitioning from "cool" to "neutral", namely, the corresponding TCL and RTS are "cozy" and "hotter", respectively, and the TTCL will be "cozy to hot". However, since the "neutral" ATS is cozier than the "cool" ATS, intuitively, the TTCL should be "cold to cozy" but not "cozy to hot". However, it is not that big of a deal. We can simply solve this problem by redefining the "cozy" TCL to exclusively contain the "neutral" ATS. In fact, in this study, to reduce the error caused by the subjects' subjectivity as well as to increase the stability, the "cozy" TCL was regarded to include a broader range covering the ATS of "warm", "neutral", and "cool". After the transformation from the ATS to the TCL, the internals in the original ATS could be neglected.

Thirdly, the instance segmentation-based feature extraction method can only work under the condition that the users wear similar clothes to the original one used to gather data and train the model. If the users change their clothes significantly (e.g., from short sleeves to cotton coat), the trained model might never be valid. However, we can solve this problem by training several corresponding models for one individual wearing several typical clothes. Alternatively, we can use head segmentation algorithms instead to obtain the occupants' head thermal profiles to solve this problem since the head is not covered by the clothes.

Fourthly, as this study is focused on the personalized assessment of thermal comfort and belongs to non-statistical analysis, a relatively small subject sample size (six young male subjects) was adopted. Even though the results are significant, a larger subject sample size and additional investigation on aged people would enhance the validity of the results.

Lastly, though the gradual heating phase, the rapid and gradual cooling phases were simulated in the experiment, the rapid heating phase was not investigated in this study.

5. Conclusions

In this paper, we investigated the concept of RTS by merely adding two additional RTSVs (“hotter” and “colder”) to a conventional thermal sensation scale (7-point ATSS). The RTS forms a new branch of the thermal comfort theory and bridges the gap for the assessment of thermal sensation trend in the field of thermal comfort, which brings new insight for transient-state thermal comfort assessment since the RTS can provide ordinary thermal comfort models with another dimension to enhance them by forming composite thermal comfort models. Then, we investigated the intrusive and non-intrusive methods for real-time RTS assessments. The RTS does not always comply with the current ambient air temperature trend but can also be influenced by the previous context. By integrating the 3-point RTSS into the 3-point TCS, the 9-point TTCS was derived, which is capable of both predicting the current thermal comfort and the current thermal sensation trend and can provide an early warning mechanism and a deterioration prevention mechanism for thermal discomfort. We used the MLP classification algorithm to assess the subjects’ personal real-time RTS and TCL. Additional findings that were not reported in our preliminary work [32] are illustrated as follows: (1) the LBPT, the gradients of the LBPT, the DRTP, and the gradients of the DRTP have been shown to be relevant for RTS modeling; (2) the LBPT, gradients of the LBPT, and the DRTP have been shown to be relevant for TCL modeling; (3) in addition to the thermal discomfort early warning system, the TTCL also has a thermal discomfort deterioration prevention mechanism; (4) for the TTCL assessments, the intrusive method outperformed the non-intrusive method; (5) for the intrusive method of the TTCL using the LBPT features, the mean accuracy reached 59.7% and 52.0% in Scenarios I and II, respectively, which is much higher than that in our preliminary work [32]; for the non-intrusive method of the TTCL using the DRTP features, the mean accuracy reached 45.3% and 42.7% in Scenarios I and II, respectively. This pilot study facilitates practical applications for thermal discomfort early warning systems and deterioration prevention systems and contributes to energy conservation in buildings.

CRediT authorship contribution statement

Ziyang Wang: Conceptualization, Methodology, Writing – original draft, Writing – review & editing. **Ryuji Matsuhashi:** Project administration, Funding acquisition, Supervision. **Hiroshi Onodera:** Software, Visualization.

Declaration of competing interest

The authors declare that they have no known competing financial interests or personal relationships that could have appeared to influence the work reported in this paper.

Data availability

The data that has been used is confidential.

Acknowledgments

The authors would like to acknowledge our partners Aizawa-san and Yokoyama-san from Tokyo Gas Co., Ltd., for their wonderful collaboration, useful discussions, and suggestions.

References

[1] Agency IE. Buildings – topics - IEA. 2020, https://www.iea.org/topics/buildings. [Accessed: 2021-8-30].
[2] Agency IE. The future of cooling. 2020, https://www.iea.org/reports/the-future-of-cooling. [Accessed: 2021-8-30].
[3] Ashrae. ANSI/ASHRAE standard 55-2017 : Thermal environmental conditions for human occupancy. vol. 2017, ASHRAE Inc.; 2017, p. 66.
[4] Luo M, Cao B, Zhou X, Li M, Zhang J, Ouyang Q, et al. Can personal control influence human thermal comfort? A field study in residential buildings in China in winter. Energy Build 2014;72:411–8.
[5] Choi JH, Yeom D. Study of data-driven thermal sensation prediction model as a function of local body skin temperatures in a built environment. Build Environ 2017;121:130–47.
[6] Velt KB, Daanen HAM. Thermal sensation and thermal comfort in changing environments. J Build Eng 2017;10(February):42–6.
[7] Ranjan J, Scott J. ThermalSense: Determining dynamic thermal comfort preferences using thermographic imaging. In: UbiComp 2016 - proceedings of the 2016 ACM international joint conference on pervasive and ubiquitous computing. 2016, p. 1212–22.
[8] Ghahramani A, Castro G, Karvigh SA, Becerik-Gerber B. Towards unsupervised learning of thermal comfort using infrared thermography. Appl Energy 2018;211(October 2017):41–9.
[9] Li D, Menassa CC, Kamat VR. Non-intrusive interpretation of human thermal comfort through analysis of facial infrared thermography. Energy Build 2018;176:246–61.
[10] Cosma AC, Simha R. Thermal comfort modeling in transient conditions using real-time local body temperature extraction with a thermographic camera. Build Environ 2018;143(June):36–47.
[11] Fanger PO, et al. Thermal comfort. Analysis and applications in environmental engineering. 1970.
[12] Wang Z, de Dear R, Luo M, Lin B, He Y, Ghahramani A, et al. Individual difference in thermal comfort: A literature review. Build Environ 2018;138:181–93.
[13] Takada S, Matsumoto S, Matsushita T. Prediction of whole-body thermal sensation in the non-steady state based on skin temperature. Build Environ 2013;68:123–33.
[14] Fiala D. Dynamic simulation of human heat transfer and thermal comfort. Sustain Dev 1998;45(2001):1.
[15] Zhang H. Human thermal sensation and comfort in transient and non-uniform thermal environments [Ph.D. thesis], Berkeley ProQuest Dissertations Publishing, University of California; 2003.
[16] Schellen L. Beyond uniform thermal comfort: on the effects of non-uniformity and individual physiology [Ph.D. thesis], research.tue.nl, Technische Universiteit Eindhoven; 2012.
[17] Uğursal A, Culp CH. The effect of temperature, metabolic rate and dynamic localized airflow on thermal comfort. Appl Energy 2013;111:64–73.
[18] Yao Y, Lian Z, Liu W, Jiang C, Liu Y, Lu H. Heart rate variation and electroencephalograph - The potential physiological factors for thermal comfort study. Indoor Air 2009;19(2):93–101.
[19] Yang S, Wan MP, Chen W, Ng BF, Dubey S. Model predictive control with adaptive machine-learning-based model for building energy efficiency and comfort optimization. Appl Energy 2020;271:115147.
[20] Nkurikiyeyezu KN, Suzuki Y, Lopez GF. Heart rate variability as a predictive biomarker of thermal comfort. J Ambient Intell Humaniz Comput 2018;9(5):1465–77.
[21] Huizenga C, Zhang H, Arens E, Wang D. Skin and core temperature response to partial- and whole-body heating and cooling. J Therm Biol 2004;29(7):549–58.
[22] Wang X. Thermal comfort and sensation under transient conditions [Ph.D. thesis], KTH Royal Institute of Technology; 1994.
[23] Charkoudian N. Skin blood flow in adult human thermoregulation: how it works, when it does not, and why. Mayo Clin Proc 2003;78(5):603–12.
[24] Kellogg Jr. DL. In vivo mechanisms of cutaneous vasodilation and vasoconstriction in humans during thermoregulatory challenges. J Appl Physiol 2006;100(5):1709–18.
[25] Zhang H, Arens E, Huizenga C, Han T. Thermal sensation and comfort models for non-uniform and transient environments: Part I: Local sensation of individual body parts. Build Environ 2010;45(2):380–8.
[26] Zhang H, Arens E, Huizenga C, Han T. Thermal sensation and comfort models for non-uniform and transient environments, part II: Local comfort of individual body parts. Build Environ 2010;45(2):389–98.

[27] Zhang H, Arens E, Huizenga C, Han T. Thermal sensation and comfort models for non-uniform and transient environments, part III: Whole-body sensation and comfort. Build Environ 2010;45(2):399–410.
[28] Hastings S, Kim SW, Brown RD. Face temperature as an indicator of thermal stress in outdoor work environments. Atmosphere 2020;11(6):627.
[29] Li D, Menassa CC, Kamat VR. Robust non-intrusive interpretation of occupant thermal comfort in built environments with low-cost networked thermal cameras. Appl Energy 2019;251(April):113336.
[30] Li D, Menassa CC, Kamat VR, Byon E. HEAT - human embodied autonomous thermostat. Build Environ 2020;178:106879.
[31] Cosma AC, Simha R. Machine learning method for real-time non-invasive prediction of individual thermal preference in transient conditions. Build Environ 2019;148:372–83.
[32] Wang Z, Onodera H, Matsuhashi R. Proposal of relative thermal sensation: Another dimension of thermal comfort and its investigation. IEEE Access 2021;9:36266–81.
[33] Gilani SIUH, Khan MH, Pao W. Thermal comfort analysis of PMV model prediction in air conditioned and naturally ventilated buildings. Energy Procedia 2015;75:1373–9.
[34] Jiang SC, Ma N, Li HJ, Zhang XX. Effects of thermal properties and geometrical dimensions on skin burn injuries. Burns 2002;28(8):713–7.
[35] Kashcooli M, Salimpour MR, Shirani E. Heat transfer analysis of skin during thermal therapy using thermal wave equation. J Therm Biol 2017;64:7–18.
[36] huehuehuehue. Anatomy human body human back back pain clip art - PNG - download free. In: FAVPNG.Com. 2017, https://favpng.com/png_view/anatomy-human-body-human-back-back-pain-clip-art-png/bJFf3LQh, [Accessed: 2022-1-21].
[37] Bolya D, Zhou C, Xiao F, Lee YJ. Yolact: Real-time instance segmentation. In: Proceedings of the IEEE international conference on computer vision. openaccess.thecvf.com; 2019, p. 9157–66.
[38] Bolya D, Zhou C, Xiao F, Lee YJ. YOLACT++: Better real-time instance segmentation. IEEE Trans Pattern Anal Mach Intell 2020;PP.
[39] Van Der Maaten L, Postma E, Van den Herik J. Dimensionality reduction: a comparative review. J Mach Learn Res 2009;10(66–71):13.
[40] Guo X, Liu X, Zhu E, Yin J. Deep clustering with convolutional autoencoders. In: Neural information processing. Springer International Publishing; 2017, p. 373–82.
[41] McInnes L, Healy J, Melville J. UMAP: Uniform manifold approximation and projection for dimension reduction. 2018, ArXiv e-prints.
[42] Bergmeir C, Benítez JM. On the use of cross-validation for time series predictor evaluation. Inform Sci 2012;191:192–213.
[43] Wainer J, Cawley G. Nested cross-validation when selecting classifiers is overzealous for most practical applications. Expert Syst Appl 2021;182:115222.
[44] Chaudhuri T, Zhai D, Soh YC, Li H, Xie L. Thermal comfort prediction using normalized skin temperature in a uniform built environment. Energy Build 2018;159:426–40.
[45] Wang Z, Matsuhashi R, Onodera H. Pilot study on early warning systems for thermal discomfort using body surface temperature for energy conservation in the building sector. 2021, https://www.energy-proceedings.org/wp-content/uploads/icae2021/1644391188.pdf. [Accessed: 2022-4-11].